



Effect of Slip-Weakening Distance on Seismic–Aseismic Slip Patterns

PIOTR SENATORSKI¹

Abstract—In order to explain the seismic–aseismic slip patterns observed on megathrust faults, numerical simulations were carried out using the quasi-dynamic asperity fault model with the slip-dependent friction and stress-dependent healing. Two friction law parameters, strength and slip-weakening distance, are interpreted in the subduction channel context. The parameters are treated as random fields with specified characteristics. Their distributions define heterogeneities of the interplate frictional coupling. The higher strength regions accumulate stresses, whereas the slip-weakening distance lengths control the stress release rates. The simulation results indicate that the slip-dependent asperity model reproduces key features of real megathrust fault behavior. First, stable and unstable slip movements can occur at the same locations, even if the friction parameters are fixed. Second, two rupture styles, single asperity breaks and wide, smooth, propagating rupture fronts, can be distinguished. The latter style is responsible for large slips near the free surface, where lower fault strengths are expected. The reason for these effects is that slip instabilities depend both on local friction and on the system stiffness, which is related to the slipping area size and distribution of slips. It is also shown that the high-strength interplate patches, such as subducted seamounts, can both promote and restrain large earthquakes, depending on the slip-weakening distance lengths.

Key words: Earthquake dynamics, slip-dependent friction, slow and fast slip, numerical modeling, subduction zone processes, megathrust earthquakes.

1. Introduction

Slip movements on the subduction interface can be considered in terms of the slip budget. At any point, the long-term slip is controlled by the plate convergence rate, V_p . The slip deficit is accumulated over a period of time in a given region, if the slip rate is lower than the convergence rate. The slip deficit is released by both seismic and aseismic slips, which

complement each other on the plate interface. Understanding of the interplay between fast and slow slips, such as regular earthquakes and slow slip events (Peng and Gomberg 2010), respectively, is crucial for earthquake hazard estimations.

The interplate coupling coefficient is defined as the ratio of the slip deficit rate over the plate convergence rate. Regions of high interseismic coupling roughly correspond with high-coseismic-slip regions in most cases (Moreno et al. 2010, 2012; Hashimoto et al. 2012; Loveless and Meade 2011).

A general approach towards the seismic and aseismic slip interplay is given by asperity fault models. Such models assume that the fault plane consists of strong patches of episodic, unstable slips, which are surrounded by weaker, creeping regions (Lay et al. 1982). The slow slips in the non-asperity regions concentrate stresses in the asperity regions during interseismic periods. Asperities accumulate stresses until they break during earthquakes. More sophisticated models assume hierarchical asperity structures (Uchida and Matsuzawa 2011; Ohtani et al. 2014).

Fast and slow slips are commonly interpreted in terms of frictional fault characteristics, with asperities and non-asperity regions treated as fixed, spatially separated fault features. That view is inconsistent with observations of the Tohoku–Oki 2011 earthquake. First, the largest coseismic slip occurred in the shallow fault area considered to be a velocity-strengthening and slowly creeping region (Ide et al. 2011). Second, aseismic afterslip occurred within the areas of previous smaller earthquakes considered to be velocity-weakening asperities (Johnson et al. 2012). Explanations of these inconsistencies, or the slow and fast slip paradox, can refer to the applied friction law modifications (Noda and Lapusta 2013), non-planar fault geometry (Fukuyama and Hok

¹ Institute of Geophysics, Polish Academy of Sciences, ul. Księcia Janusza 64, 01-452 Warsaw, Poland. E-mail: psenat@igf.edu.pl

2013), or rupture dynamics and free surface effects (Huang et al. 2013).

The present paper refers to fault heterogeneities and the system stiffness to solve the problem. Stability of the slip movement at a given location depends both on the local friction characteristics and the rate at which the resisting stress decreases with the ongoing slip, i.e., on the critical stiffness, and on the rate at which the driving stress changes with the ongoing slip, i.e., on the system stiffness (Senatorski 2002; Mansinha and Smylie 1971). The latter factor changes with time since distribution of slips, which contribute to the driving stress, evolves in time. The proposed model enables us to explain the observed fault behavior without introducing any extra, velocity-dependent, weakening mechanism to the friction law.

Spatial variations of the interplate frictional coupling are considered in terms of the asperity fault model. Structural and material heterogeneities along the fault plane, due to subducted seamounts, oceanic ridges, sediments, and released fluids, are thought to be responsible for the coupling variations. The specific role of subducted seamounts or sediments have been debated (Wang and Bilek 2011; Scholz and Campos 2012; Heuret et al. 2012). It is not clear, whether the seamounts start or stop large earthquakes (Wang and Bilek 2011).

In the present paper, topographic features are modeled by slip-dependent cohesive stresses acting along the fault plane. The cohesive stress is defined at each point of the fault plane as a function of slip by two parameters: the peak stress or fault strength, and the slip-weakening distance at which friction or cohesive stress decreases to its residual level. The strength can be related to the normal stress variations due to the hilly topography of the subducting plate surface (Scholz and Small 1997). The slip-weakening distance can be related to the material fault characteristics, such as subducted sediment layers or fluids (Heuret et al. 2012; Vannucchi et al. 2017). Thus, variations of the interplate frictional coupling are defined as distributions of these two parameters. The first aim is to relate these distributions to the stable and unstable slip patterns. The second aim is to find out whether such distributions promote small or large earthquakes.

A subduction zone plate interface is a subduction channel hundreds of meters to several kilometers thick, lubricated by a layer of shearing unconsolidated sediment (Cloos and Shreve 1988; Vannucchi et al. 2012). Consequently, assumed friction or cohesive stress variations applied to the model fault plane approximate all processes taking place in the channel: not only sliding along a well-defined thin rupture plane, but also sediment viscous flow dragged by the descending plate, the sediment dewatering, consolidation and underplating to the hanging wall, the upper plate erosion and seamounts being jammed against the roof of the thinning channel (Cloos and Shreve 1996). Therefore, fault strength and slip-weakening distance parameters, as well as the shear stress critical value for slip healing described below, even if well-supported by laboratory experiments with the sliding friction (Ohnaka and Shen 1999; Brantut 2015), here are also interpreted within the subduction channel context.

To study seismic–aseismic slip patterns, long-term fault dynamics and a large range of spatial and temporal scales should be modeled. To that end, quasi-dynamic fault models have been used for computer simulations by many authors as the optimal solution (Rice 1993; Senatorski 1995, 2002; Ziv and Cochard 2006; Hillers et al. 2006; Ohtani et al. 2014; Ohtani and Hirahara 2015). Such models enable us to generate realistic, both slow and fast, slip movements. It should be borne in mind, however, that details of coseismic slips obtained from quasi-dynamics can differ from those obtained from fully dynamic models. The difference depends on the friction law applied and related fault rupture style (Thomas et al. 2014).

In its general form, the present model is similar to other models based on the quasi-dynamic approximation. Other authors (Hillers et al. 2006) investigated the spatially variable critical slip distance and the resultant complexity in seismicity patterns, using the model based on rate-and-state friction law. The main difference between their approach and the present one concerns details of the interplate frictional coupling formulation, including the applied friction law and distribution of its parameters, which defines asperity and non-asperity regions on the megathrust fault.

The model used in the present work is similar to the model described in the previous work (Senatorski 2002). The main objective of this paper concerns the relation between the megathrust fault structural and material characteristics and the slow and fast slip interplay, so the model is adapted to megathrust seismicity context. Its formulations of slip-dependent friction or cohesive stress, healing and asperity distributions, interpreted in the context of subduction channel processes, enable us to find an explanation of the slow and fast slip paradox mentioned above, as well as the role of subducted seamounts as both promoting and restraining large earthquakes.

2. Methods

2.1. Theory

Geometry An earthquake source is modeled as a planar cut in an elastic half-space subjected to the background tectonic shear stress, s^T . An earthquake rupture process is represented by evolution of stresses and slip displacements, $s(\mathbf{r}, t)$ and $q(\mathbf{r}, t)$, respectively, defined over the rupture area, A , and the earthquake slip duration, T . For simplicity, only one component of slips and shear stresses defined on a planar fault, the subducting direction component, is considered. Distributions of slips and stresses change from $q(\mathbf{r}, t = 0)$ to $q(\mathbf{r}, t = T)$ and from $s(\mathbf{r}, t = 0)$ to $s(\mathbf{r}, t = T)$, respectively, during the earthquake. The slip movement gradually reduces the stress to the residual value of the cohesive or frictional resistance, s^F .

Quasi-dynamics. The quasi-dynamic evolution equations for slips can be derived in two steps. First, the stress pulse, $\Delta s = s^T - s^F$, is applied over the $z = 0$ fault plane instantaneously at $t = 0$ (Brune 1970). Second, the resulting equation is generalized to the heterogeneous rupture case by introducing the interaction stress term, s^I . Assume that the uniform stress pulse propagates along the z -axis perpendicular to the fault plane at the shear wave speed, v_S .

$$\frac{\mu}{2v_S} \dot{q}(\mathbf{r}, t) = \Delta s(\mathbf{r}, t) = s^T + s^I(\mathbf{r}, t) - s^F(\mathbf{r}, t), \quad (1)$$

where μ is the shear modulus, $s = s^T + s^I$ is the driving stress, s^F is friction or the cohesive stress, and

Δs represents the net stress. In that approximation, the radiated energy can be illustrated as the area between the driving and frictional or cohesive stress lines in the stress vs. slip plots (Senatorski 2002). Equation (1) represents the instantaneous radiation of a plane wave from the fault when the shear stress is released. Its left-hand side can be interpreted as the radiational stress, with the mechanical impedance, $\kappa = \mu/v_S$, i.e., ratio of the stress and the particle velocity, $\dot{q}/2$ (Achenbach 1975). The same equation has been derived rigorously as the overdamped dynamics (Senatorski 1994, 1995) from the energy functional (Rundle 1989), from the stress balance (Rice 1993), or from the full dynamics by assuming that stress transfer is instantaneous (Cochard and Madariaga 1994) in the two-dimensional (2D) case. For the assumed one component of slip and shear stress, its general form is the same in the three-dimensional (3D) case.

Interactions. The interaction stress describes the long-range elastic interactions along the fault plane. It is due to heterogeneities of the slip field. It is expressed as

$$s^I(\mathbf{r}, t) \approx \int_A d\mathbf{r}' G(\mathbf{r}, \mathbf{r}') q(\mathbf{r}', t), \quad (2)$$

where A is the rupture area, and function $G(\mathbf{r}, \mathbf{r}')$ represents the static stress at point \mathbf{r} due to unit slip at point \mathbf{r}' . It is assumed that (1) the wavefront at $|\mathbf{r} - \mathbf{r}'| = t \cdot v_S$ simply leaves the static stress field behind it, so variations of the transient stress between the longitudinal and transverse wavefronts are neglected (Hirth and Lothe 1967); and (2) that effects of finite wave speed, or the stress correction due to the stress signal delay, are neglected. Such an approximation enables us to express stresses in terms of slips at the same instead of at earlier instants, which defines the overdamped or quasi-dynamics. The meaning and validity of the approximation are discussed in Senatorski (2014).

Function G depends on the system geometry. For simplicity, the vertical fault in a half-space solution, with vertical slip direction, is used in the present work. Consequently, the attractive force between slips and a free surface is taken into account, but effects of a fault dip angle value are ignored. In particular, the normal stress variations, which are

responsible for the fault strength (Scholz and Campos 2012), are not considered. Instead, the fault strength is introduced directly by defining cohesive stresses, s^F , acting along the fault plane. Such an approach enables us to study effects of the cohesive stress parameters, such as strength or slip-weakening distance, for megathrust fault seismicity. The Green's function G used in previous works (Senatorski 2002, 2004) has been adapted to the simplified megathrust geometry by changing fault boundary conditions. It is consistent with the solutions presented by other authors (Chinnery 1963; Mansinha and Smylie 1971; Okada 1992).

Cohesive stress. The cohesive stress field, s^F , is defined at each point of the fault interface as a Gaussian function of the slip displacement from the previous event, or the last healing, $\tilde{q}(\mathbf{r}, t)$,

$$s^F(\tilde{q}) = \frac{b}{d}(\tilde{q} + \alpha d) \exp\left\{0.5 - \frac{(\tilde{q} + \alpha d)^2}{2d^2}\right\}, \quad (3)$$

where b represents the cohesive stress peak, d represents the slip-weakening distance, and α is related to the initial stress: for $\alpha = 0$, the initial stress is zero and it attains the peak value b for $\alpha = 1$ (Fig. 1). For $\alpha < 1$, the cohesive stress increases with increasing slip until its peak value is attained, then it decreases with the ongoing slip to the residual value assumed as zero. Here, $\alpha = 0.6$ is assumed in simulations. The peak stress, $b(\mathbf{r})$, defines the fault strength at a given point \mathbf{r} . The higher the peak is, the higher stress is needed to break the site. The slip-weakening distance, $d(\mathbf{r})$, is responsible for frictional fault behavior at \mathbf{r} . The fracture energy is represented by the area under the cohesive stress line. Therefore, for a given strength, larger d implies that more fracture energy is consumed when the site moves. Small d implies sudden stress drop and higher slip acceleration, whereas its larger value implies that the stress is gradually released. These two cases can be related to intact rock failure and frictional sliding, respectively (Ohnaka 2013). The choice of the Gaussian function is motivated by the fact that it exhibits basic characteristics of the cohesive stress, with the stress peak separating its slip-strengthening and slip-weakening parts.

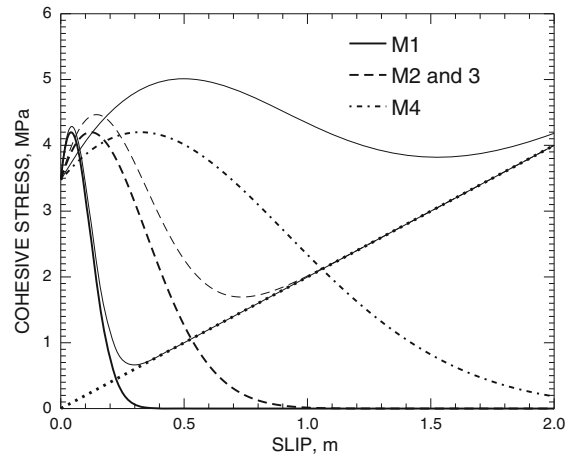


Figure 1

Illustration of a slip-dependent friction law and its stability regimes for models M1–4. Cohesive stress vs. slip displacement relations for four models are characterized by peak stresses and the slip displacements at which the peak stresses are attained (thick lines). The residual friction stress is zero. The area under the curve gives density of the fracture energy consumed by the cohesive forces. The back stress, kq , due to the elastic medium response for the case of uniform slip along a square patch (the rest of the fault unmoved), is determined by the system stiffness, $k \approx 8/L$ [MPa/m], where L is the patch size in kilometers (dotted line; $L = 4$ km is assumed). The resisting stress is defined as a sum of the cohesive stress and the back stress (thin lines)

Healing mechanism. After the driving stress drops below the healing stress level, $s < s_H$, the slip movement stops and the cohesive stress is instantaneously rebuilt, i.e., $\tilde{q} \rightarrow 0$ and $s^F \rightarrow s^F(\tilde{q} = 0)$. The healing stress is assumed to be proportional to the peak stress, $s_H = \beta b$, with $\beta = 0.1$. Then, when the driving stress attains the cohesive stress initial value, $s > s^F(0)$, s^F starts to increase and, after attaining its peak value, $s^F = b$, to decrease with the increasing slip, according to Eq. (3), till the next healing. Note that the healing mechanism activation occurs at low driving stress level, when the slip velocity is low too. Therefore, the healing is not activated shortly after the slip begins, when the slip velocity is low, but the driving stress is high. The model behavior depends on the healing parameter β : Its lower value smooths out heterogeneities in slips on the fault after consecutive earthquakes, which leads to more regular earthquake cycles. In fact, transition from regular behavior ($\beta = 0.04$) through period doubling ($\beta = 0.06$) to chaos ($\beta = 0.1$) has been observed in simulations with constant slip-weakening distances (Senatorski

2002). On the other hand, a larger β would lock slipping at too high rates, so $\beta = 0.1$ is here assumed as generating realistic slip patterns.

The abrupt arrest of seismic slip at a given point can be interpreted as the effect of the short-scale variations of the dynamic friction above its residual value, due to, for instance, encountered small asperities. For low enough driving stress, such varying resistance locks the movement locally at the final value of sliding friction higher than its residual value (Brune 1976). The resistance variation level is assumed to be related to the local fault strength. The healing stress, s_H , can be regarded as the upper limit of the size of the variations. The chosen $\beta = 0.1$ value means that the upper limit of the variations is 10 percent of the local strength, b . Here it is assumed that the slip movement stops with probability 1 if the driving stress drops below the s_H level.

The proposed healing mechanism, despite its simplifications, leads to realistic fault behavior: local stress and slip velocity variations, rupture propagation, earthquake parameters, and seismic cycle complexity, are similar, at least qualitatively, to those estimated for real seismicity or laboratory experiments (Senatorski 2002, 2006). Note that (1) the mechanism operates when the local slip velocity decreases; (2) there is no healing if high driving stresses overcome high cohesive stresses, i.e., restrengthening occurs after the stresses at a point had been mostly released. On the other hand, the mechanism causes an instantaneous increase of the cohesive stress to its initial value after healing. Note, however, that (3) the healing rule is local. The collective behavior of larger fault patches is more complicated: strengths of the locked patches depend on their size and distribution of strengths in their surroundings, so it changes gradually with the rupture extension.

Subduction channel Slips along a thin fault plane actually represent deformations within a subduction channel, or a subduction interface that is hundreds of meters to several kilometers thick (Cloos and Shreve 1988). Natural heterogeneities, such as the seafloor topography and subduction channel material characteristics, are mapped as distributions of the cohesive stress parameters. Thus, the cohesive stress concept can be thought of as representing all subduction

channel processes and characteristics, including variations of normal stresses due to the plate topography, pore pressure and buoyancy of the subduction channel material, sediment consolidation, its viscosity and density, as well as the channel thickness. Seamounts and other topographic features within the channel, which is filled with sediments and fluids, create a complicated structure. Its detailed and realistic description in terms of a hilly surface moving across the non-elastic medium requires an adequate theory. Using the cohesive stresses as representing basic, averaged characteristics of the subduction channel, including both slip along rupture planes and volume deformations within the channel, is chosen as an alternative approach. Note that horizontal dimensions of the topographic features, such as seamounts, are of an order of kilometers, whereas earthquake slips are measured in meters, so the related strength heterogeneities can be treated as fixed characteristics.

Also, threshold stress for healing can be interpreted in the subduction channel context. Sediment dewatering and underplating can not occur where the shear stress acting on the material near the channel roof exceeds a critical value. On the other hand, strong asperities, such as seamounts, can still slowly move with the descending plate where the shear stress is high enough to rasp the overriding plate, causing its erosion (Cloos and Shreve 1988). The proposed model suggests that two processes should be distinguished: frictional sliding, and underplating or erosion processes. The latter is related to enabling or inhibiting the healing mechanism. That is why the slip-dependent cohesive stress and the healing mechanism are treated separately in this approach.

Tectonic stress The tectonic stress, s^T , is due to the tectonic loading,

$$s^T = s^T(t_0) + \frac{\mu}{w} \left\{ V_P(t - t_0) - \frac{1}{A} \int_A d\mathbf{r} [q(t, \mathbf{r}) - q(t_0, \mathbf{r})] \right\}, \quad (4)$$

where V_P is the relative plate velocity; t_0 means the simulation starting time; w denotes the width of the elastic medium layer surrounding the fault, as measured perpendicularly to the fault plane (Senatorski 2002). The tectonic stress increases as within the elastic layer of width w , which is deformed by a

steady movement of its sides at the relative speed V_p . Here $w = 30\text{km}$ is assumed in the simulations. The tectonic stress decreases with the mean slip along the planar cut within the layer. The stress s^T can be thought of as the uniform component of driving stresses.

Stable and unstable slips The unstable slip movements start if the driving stress, $s = s^T + s^I$, decreases slower than friction, s^F , during sliding. Consider the uniform slip q on the $L \times L$ square fault patch. In this case, the interaction stress is the back stress due to the elastic medium response, which resists the slip movement; it depends on the slipping area size. The driving stress is

$$s = s^T - k_R q, \quad (5)$$

where s^T is assumed to be constant. The driving stress decrease with increasing slip, due to the medium response or the back stress, is represented by the interaction stress term, $s^I = -k_R q$, where the system stiffness is (Senatorski 2002; Okada 1992)

$$k_R = (\mu/4\pi)[(2 - \nu)/(1 - \nu)](\sqrt{2}/L). \quad (6)$$

This gives for the back stress $k_R q \approx 8q/L$ for $\mu = 3 \times 10^4$ MPa and the Poisson's ratio, $\nu = 0.25$ (L in kilometers, q in meters; Fig. 1).

The cohesive stress decrease can be approximated as

$$s^F \approx b - k_C q, \quad (7)$$

where b denotes the cohesive stress peak value. The slip movement starts when the tectonic stress attains the cohesive stress peak stress or strength value, $s^T = b$. The critical stiffness, k_C , is proportional to the rate of the cohesive shear stress decrease,

$$k_C \approx b/d. \quad (8)$$

Both parameters, b and d , represent material fault characteristics.

The stable to unstable slip transition occurs after the system stiffness exceeds its critical value, $k_R < k_C$. The stiffness k_R depends on distribution of slips, or the area of possible slip (it is easier to move larger rupture area), whereas the critical stiffness is related to the plate frictional coupling or cohesive stress dependence on slip displacement (it increases with

the increasing slope of the stress vs. slip-weakening distance line). The critical stiffness can be exceeded in two ways: (1) by decrease of the system stiffness k_R (dynamical factor), or (2) by increase of the critical stiffness k_C (material or structural factor).

The unstable rupture condition, $k_R < k_C$, can be written as

$$L > (\mu/4\pi)[(2 - \nu)/(1 - \nu)](\sqrt{2}(d/b)). \quad (9)$$

Thus, for given strength, larger d requires larger slipping area size for an unstable rupture. In general, stable or unstable slip movements depend on distribution of slips and on the concurrently slipping area size, as well as frictional or cohesive stress local characteristics.

Figure 1 illustrates the condition for the unstable slip. For the same strength, $b = 4.2$ MPa, three cases of small (M1, $d \approx 0.2$ m), medium (M2 and M3, $d \approx 0.6$ m) and large (M4, $d \approx 1.7$ m) slip-weakening distances are considered. The critical stiffness values are, respectively $k_C = b/d = 21$ MPa/m, 7 MPa/m, and 2.5 MPa/m. The system stiffness due to the medium back stress response, represented by the $k_R q = -s^I$ dotted line, is $k_R = 2$ MPa/m ($L = 4\text{km}$), so $k_R < k_C$ in all cases. For each model, M1–M4, two lines are shown: the cohesive stress, s^F (thick line), and the fault resistance line, $s^R = s^F + k_R q$ (thin line). Assuming constant tectonic stress, s^T , the difference $\Delta s = s^T - s^R = s^T + s^I - s^F$ is the net stress given by Eq. (1). Therefore, the unstable slip is possible, if the s^R line has a minimum value lower than the tectonic stress. Note that the s^R stress peak value is higher and is attained at a larger q than the s^F peak value. This effect is due to the initial slip-strengthening part of the cohesive stress function. Only stable slip movements (i.e., slips under increasing tectonic stress) would be possible for: (1) lower strength, b , (2) larger slip-weakening distance, d , or (3) smaller rupture area size, L .

Radiated energy Intensity of the fault slip movements is measured by using the radiated energy rate signal. The radiated seismic energy, E_S , can be defined as the portion of the released potential energy, W , that is not consumed by the fault resistance to slip. For quasi-dynamics, such definition

leads to the seismic energy rate expressed as (Senatorski 1994, 2014)

$$\dot{E}_S(t) = \frac{\mu}{2v_S} \int_A d\mathbf{r} \dot{q}(\mathbf{r}, t)^2. \quad (10)$$

Equation (10) can be obtained directly from Eqs. (1), (2), and (3) by noting that they represent a gradient dynamical system, or the overdamped dynamics (Lichtenberg and Lieberman 1992; Senatorski 1994, 1995). The quasi-dynamic solution for the radiated seismic energy, E_S , when applied to real slip velocity fields, $\dot{q}(\mathbf{r})$, approximates the correct, fully dynamic solution for the radiated seismic energy. The approximation can be explained as follows: Term $(\mu/2v_S)\dot{q}$ in Eq. (10) stands for the net stress, Δs , as defined by Eq. (1), whereas the correct solution depends on the static part of the net stress only. This is because the released potential energy, W , depends on the long-range elastic interactions (or concurrent slips), as they occur in Eq. (2) (Senatorski 2014).

2.2. Specific Models

Distributions of parameters $b(\mathbf{r})$ and $d(\mathbf{r})$ are generated as random fields defined by 2D stochastic processes. Two different processes are combined. The fractional Gaussian noise enables us to model a rough surface, where the Fourier coefficients of the surface elevation, A_N , are related to the corresponding wavenumbers k_N by the relation $A_N \propto k_N^{-\beta/2}$. It results from filtering a Gaussian white noise ($\beta = 0$; Turcotte 1997). The Neymann–Scott process enables us to represent larger structures. It results from clustering applied to a Poisson process, where the daughter points are scattered around the parent points (Stoyan et al. 1995). The modeled objects, or asperities, have their internal structure, as suggested by hierarchical asperity models (Uchida and Matsuzawa 2011).

Four models, M1–M4, with the same distribution of b and different distributions of d are considered (Fig. 2; Table 1). The fault surface of 100 km length and 60 km width is discretized into 1 km \times 1 km segments. The fault plane is divided into three parts, 25, 10, and 25 km of width, respectively. The fractional Gaussian noise with $\beta = 2$, $\beta = 2.8$, and

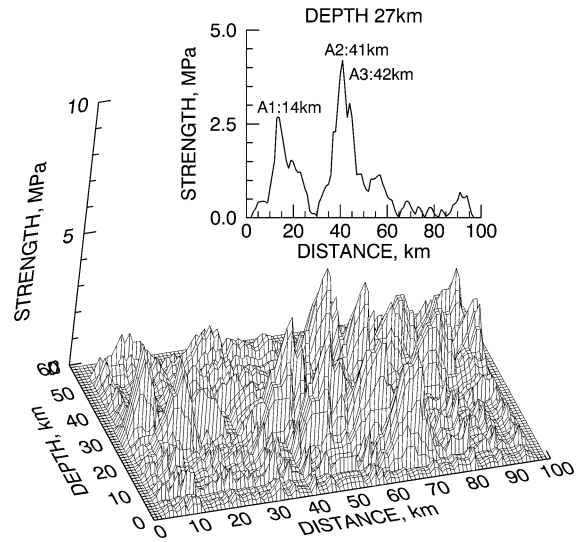


Figure 2

Distribution of peak cohesive stresses on the 100 \times 60 km² fault (with 1 \times 1 km² discretization cells). The strength random field is generated by using the combined Neymann–Scott (with maximum value of 4 MPa) and fractional Gaussian (with mean value of 0.4 MPa) stochastic processes. The 27 km at depth section with three measurement points, A1–3, is shown in the subplot. The peak stress $b = 0$ at the bottom, leftmost and rightmost boundary cells

$\beta = 0$ is applied to obtain the fault strengths, $b(\mathbf{r})$, on the deep, medium, and shallow part, respectively. Then, the Neymann–Scott process is used to create larger structures with higher strengths. The noise is rescaled, so that its mean value $b_{\text{noise}}^{\text{mean}} = 0.4$ MPa. The larger structures are rescaled, so that the maximum strength $b^{\text{max}} = 4$ MPa.

Slip-weakening distances, $d(\mathbf{r})$, are assumed proportional to the strengths, with their maximum values $d^{\text{max}} = 0.1$ m and 0.8 m for M1 and M4, respectively. If $d < d^{\text{min}}$, d is replaced by the minimum values $d^{\text{min}} = 0.02$ m for both models. For M2 and M3, $d^{\text{max}} = 0.3$ m, and the minimum values are $d^{\text{min}} = 0.01$ m. A larger value of $d^{\text{min}} = 0.4$ m is assumed in the upper 20 km layer in M3 to investigate possible effects of the higher slip-weakening distance values at smaller depth on the fault dynamics. The initial stress parameter, $\alpha(\mathbf{r})$, is fixed as $\alpha = 0.6$. Fracture energies can be obtained by integration of the cohesive stress, s^F , over slip, q . Therefore, the role of different fracture energy distributions (strengths are the same) can be analyzed by using M1–M4. Both

Table 1
Model parameters

Model	d^{\max} , m	d^{\min} , m	α	b^{\max} , MPa	b_{noise}^{\min} , MPa
M1	0.1	0.02	0.6	4	0.4
M2	0.3	0.01	0.6	4	0.4
M3	0.3	0.01, 0.4	0.6	4	0.4
M4	0.8	0.02	0.6	4	0.4

Each of the models, M1–M4, has the same distribution of strengths, b , and initial stress parameters, α . Distributions of slip-weakening distances, d , are proportional to the strengths, with scale coefficients that are different for each model. Maximum and minimum slip-weakening distances, d^{\max} and d^{\min} , maximum strength, b^{\max} , and its mean noise value, $b_{\text{noise}}^{\text{mean}}$, are given. Higher minimum critical slip (0.4 m) at the 20-km upper layer is assumed for M3

long-term seismicity and individual earthquake rupture patterns generated by the models are compared.

For a slip on a single discretization cell, $L = 1$ km, the system stiffness $k_R = 8$ MPa, so $k_R < k_C$ for M1, and $k_R > k_C$ for M2, M3, and M4. This means that spontaneous slip is possible (since the net stress increases above zero at constant tectonic stress) at a single discretization cell in the case of M1. The slip distance and slip velocity are limited during such an event: the asperity breaks, and the slip velocity pulse occurs, but it does not propagate by breaking its neighboring cells. In the case of M2, M3, and M4, the spontaneous slip is only possible if more discretization cells are involved. Small slip-weakening distances of M1 enable single, localized asperity breaking without rupture propagation. Thus, the 1 km \times 1 km discretization cell determines the smallest asperity size that can break singly, as the smallest earthquakes, or initiate larger events by rupture propagation. The assumed discretization cell size enables us to model both single asperity breaks and wide, smooth, propagating rupture fronts.

Note that estimation of the cohesive zone size for the slip-weakening friction models (Day et al. 2005) gives about 0.7 km in the case of M1, which is less than the computational grid size. This is consistent with the stiffness analysis: Single grid failures should be considered as the smallest asperity breaks. In the case of M2–M4, the estimation gives about 2 and 5 km, respectively, so well above the computational grid size.

Variations of strengths, b , correspond to topographic or structural fault characteristics, such as

seamounts and ridges. Variations of slip-weakening distances, d , correspond to frictional fault characteristics, which may be controlled by sediments or fluids. A role played by those geological features, whether they increase or decrease the interplate coupling coefficient, have been debated (Wang and Bilek 2011; Scholz and Small 1997). In the present paper, effects of related strength and friction variations are studied.

The relative plate velocity $V_P = 0.1$ m/year is assumed in Eq. (4). This value defines the long-term time scale of tectonic loading. For computational reasons, to enable simulations of both earthquake cycles (the long-term time scale in years) and single events (the short-term time scale in seconds) by using the same model, a higher impedance value of $\kappa^y = 0.001\mu$ MPa year/km = $3 \cdot 10^4$ MPa s/km is used. Then, when details of single events or multiple events are analyzed, the rescaling procedure is applied, with the scale factor $\kappa^s / \kappa^y = 0.006$ s/year, to recover the correct order of magnitude of slip rates during earthquakes (Senatorski 2002). Interpretation of the simulation results needs caution since the tectonic plate rate-to-slip rate ratio (so earthquake recurrence time to earthquake duration time) is higher in simulations than in the real world. To distinguish between multiple events and separated earthquakes, one should verify whether the event is triggered by slips at neighboring sites or by the tectonic loading (Senatorski 2002). The approach enables us, however, to analyze the seismic vs. aseismic slip interplay effectively.

Because of the model fault size, 100 km \times 60 km, up to ≈ 4 MPa strengths, earthquakes with up to

$\approx 1\text{m}$ of slip are generated at an average rate determined by a 0.1m/year slip budget.

3. Results

3.1. Long-Term Scale

The radiated energy rate variations (Fig. 3a), computed by using Eq. (10), exhibit irregular earthquake sequences. The largest events are separated by smaller ones. Time between the largest earthquakes varies, but subsequent seismic cycles can be distinguished by looking at the tectonic stress variations: New cycles start after the tectonic stress is mostly released (Fig. 3b). Thus, the tectonic stress signal provides extra information about system behavior.

Larger energy rates and largest tectonic stress drops occur for lower d^{max} (M1). Larger tectonic stresses are attained for higher d^{max} (M3), but they decrease more gradually. Larger d , or larger fracture energies, stabilize the system, causing its evolution to be gentler, even if high peak stresses are attained. Note that the higher stresses do not imply larger stress drops.

Large earthquakes can follow sequences of smaller events. Such patterns illustrate the problem of earthquake forecasting based on a short-term seismicity. In fact, the regularly repeating moderate earthquakes within the Tohoku–Oki region before the great 2011 event might have suggested that they are characteristic for the region. On the other hand, old tsunami traces suggest that much larger earthquakes

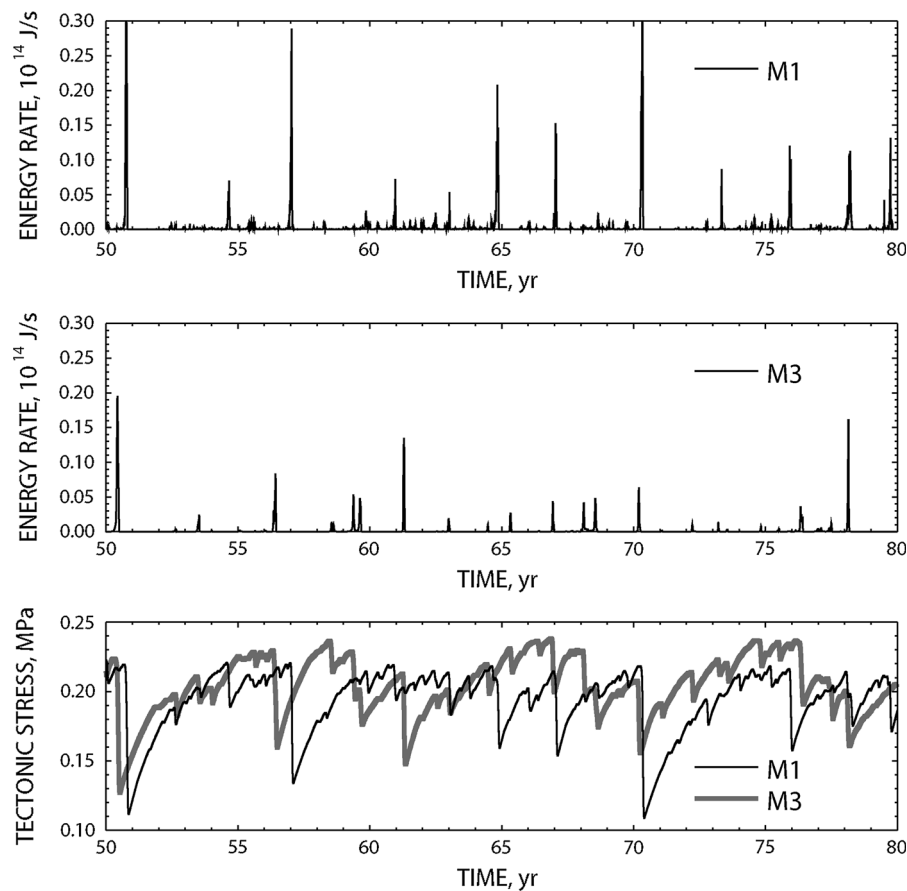


Figure 3

Long-term fault behavior. Seismic energy release rates for models M1 and M3, and time variations of the tectonic stress for the same models

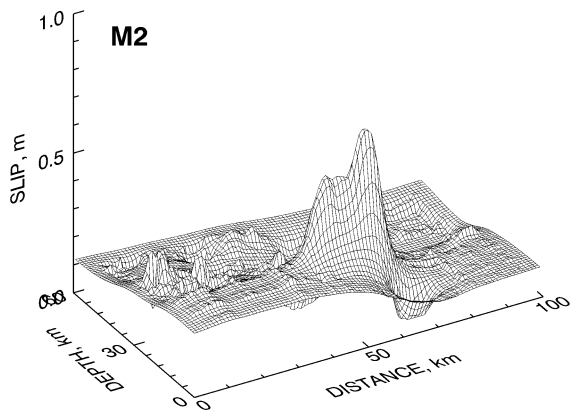


Figure 4

Distributions of slips on the fault during 1-year-long interval for the model with larger slip-weakening distances (M2): aseismic slips and coseismic slips at broken asperities

occur with the repeat time of about a thousand years (Hashimoto et al. 2012).

Both seismic and aseismic slips can be recognized in Fig. 4 (M2), where distribution of slip distances

covered during a 1-year-long interval is shown. The elevated, curved surface represents the aseismic slip of about 10–20 cm. The hills represent coseismic slips and the valleys represent coupled, slip-deficit regions. Note that the slips are measured relative to their reference distribution at a given time; the coseismic slips do not exceed the maximum aseismic slip value as measured from the beginning, zero slip distribution. In the long-term perspective, the same slip distance is covered at each point. For shorter time intervals, however, changing areas of slip deficits and excess occur around asperity regions. Although the hill and valley patterns change with time to some extent, their general outlines remain permanent fault features.

Despite slight difference between slip-weakening distance values at smaller depth for M2 and M3, general characteristics of their dynamics are similar, as determined mainly by the large structures. The difference may be essential for the resulting ground

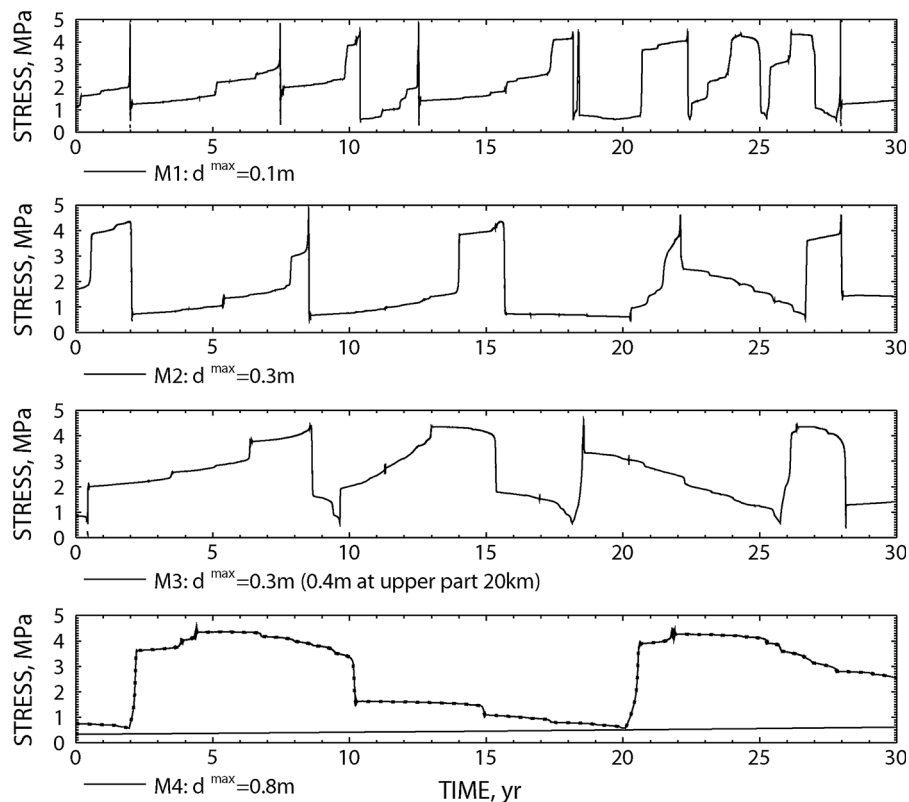


Figure 5

Driving stresses at the same asperity (41 km along strike, 27 km of depth) for M1–M4. The stresses exhibit slow increase and sudden drops for M1. Sudden stress drops related to large earthquakes are followed by slow slips for M2 and M3

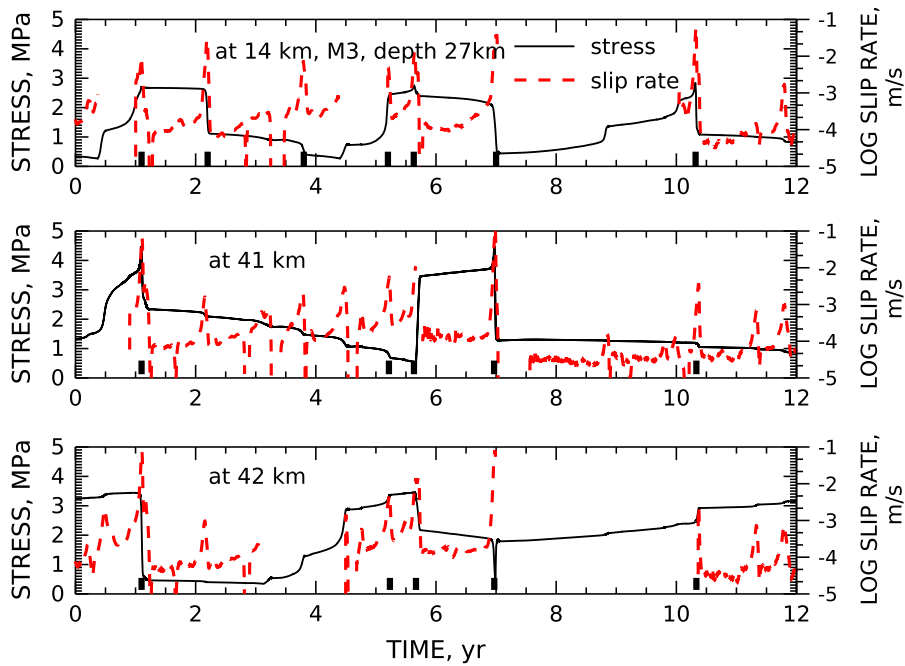


Figure 6

Driving stresses and slip rates (in log scale, dashed lined) at different asperities (A1: 14 km; A2: 41 km; and A3: 42 km along the strike, 27 km of depth) for M3. Different stress patterns between large events are shown. Fast slips during earthquakes are indicated by vertical bars. Zero slip rates mean locked asperity

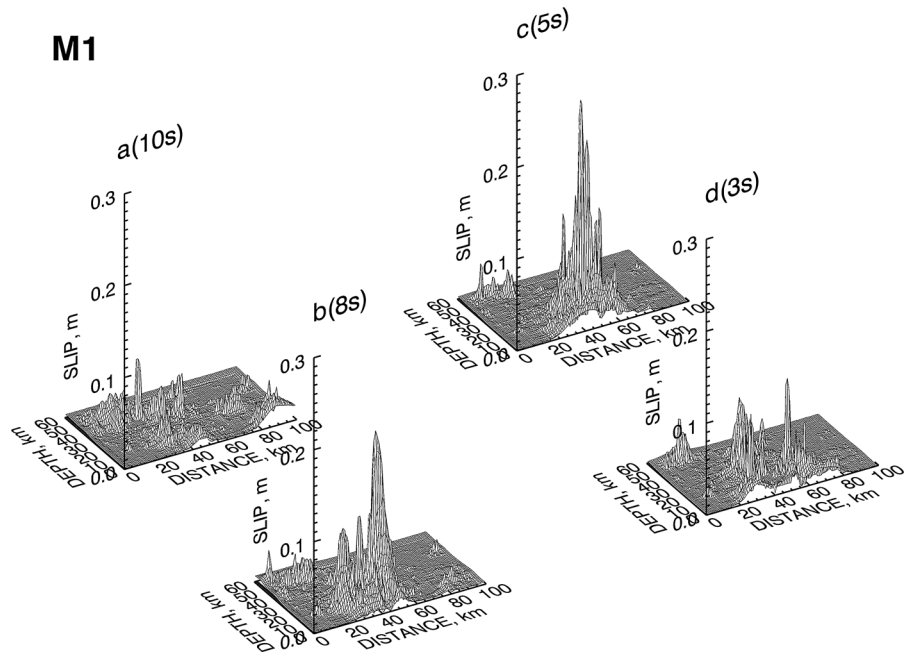


Figure 7

Distributions of slips on the fault for consecutive 3 – 10s intervals: a 0–10 s, b 11–18 s, c 19–24 s, and d 25–28 s, for the model with shortest slip-weakening distances (M1); a breaking of individual asperities; b–d propagating rupture front that activates individual asperities

motions, which is outside the scope of the present work.

3.2. Short-Term Scale

Driving stress variations at the same asperity (A2: 41 km along strike, 27 km of depth; see Fig. 2) are compared for M1–M4 (Fig. 5). The stresses increase slowly until they suddenly drop during large earthquakes for M1. For M2 and M3, steep stress drops are followed by periods of gentle stress decrease, which reflect slow slips. This means that locked asperities can exhibit both unstable, coseismic rupture and stable afterslip. Slips are more stable in the case of M4: The slip movement is too slow at the asperity to propagate into other asperities, so the area of simultaneous slip is too small for unstable movements. It can be concluded that slow and fast slip occurrences at the same place requires relatively large d , so that the unstable movement can occur only if the slipping area is adequately large.

The driving stress variations and the slip rates at different locations (A1–A3: 14, 41, and 42 km along the strike) for M2 are shown in Fig. 6. Different patterns of stress at chosen sites occur between two large events. The first event starts when A3 (42 km) breaks, inducing unstable slip at A2 (41 km). The strong asperity at 41 km exhibits fast slip during the earthquakes and slow slip between them. This slow slip increases stresses at adjacent sites, leading the next fast slip at A3, and, consequently, the sudden stress growth at A2 without its breaking. The A2 breaks later, during the second great earthquake that starts close to A1 and involves all the illustrated sites. Again, the unstable slip at 41 km occurs after the neighboring asperities become ready for being broken and, consequently, the slipping area becomes large enough. It can be concluded that both fast and slow slips are possible at the same asperity, depending on distribution of slips and stresses in its surrounding.

Distributions of slips during earthquake ruptures are illustrated in Figs. 7 and 8. Slips during consecutive several seconds-long intervals are shown. Two types of the rupture patterns can be distinguished. First, stronger patches break separately when their strengths and sizes allow unstable slip. This is

possible only if the slip-weakening distance, d , is short enough. Isolated, sharp hills representing slips that emerge from the relatively flat surface illustrate the case (Fig. 7a; M1). Second, when a larger area starts to slip, sharp peaks emerge from an extended, smooth elevation that propagates along the fault (Fig. 7b–d; M1). The strongest asperities break or re-break when the spreading slip wave sweeps them away. The unstable slip movement extends on weaker places that can slip slowly otherwise. For larger slip-weakening distance, the propagating rupture front extends, sweeping increasingly stronger asperities that cannot break separately (Fig. 8a–e; M3). Larger fault area is involved by the rupture process.

Two earthquakes simulated by using M1 ($d = 0.1$ m) and M2 ($d = 0.3$ m) are illustrated in Figs. 9 and 10, respectively. Temporal variations of the radiated energy rate are more irregular in the small d case of M1 (Fig. 9). The event consists of two subevents, which can be also treated as an earthquake doublet since slower movements occur between these subevents. The two largest asperities (A2 and A3) break almost separately during these subevents (Fig. 9c, e), with only small slips induced on the neighboring asperity. Consequently, characteristic stress switching occurs at these two asperities (Fig. 9d, f). In contrast, more regular variations of the energy rate occur in the larger d case of M2 (Fig. 10). Both asperities break during a single event (Fig. 10c), so the stress is released at both locations (Fig. 10d).

4. Discussion

The slow versus fast slip interplay is more than just about the friction law problem. This is because slip instability depends both (1) on the critical stiffness, i.e., on the local friction variations with slip, and (2) on the system stiffness, i.e., on the rate at which the driving stress decreases with slip at a given location due to the medium response. The system stiffness is related to the slipping area size and distribution of slips, so it changes from one event to another, even if the local friction parameters remain unchanged.

Computer simulations of earthquake sequences illustrate fault activity in different scales. The model

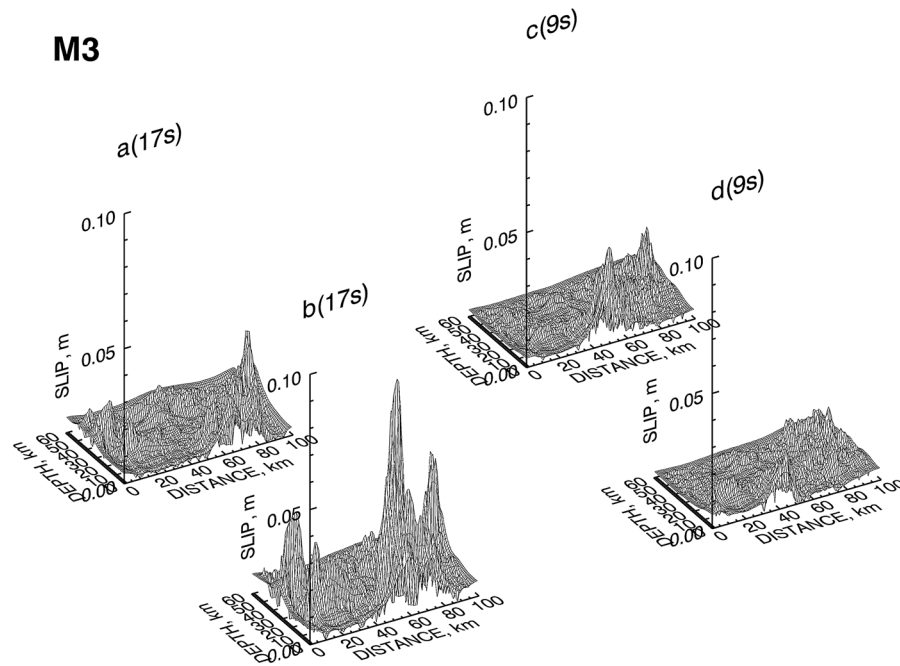


Figure 8

Distributions of slips on the fault for consecutive 9–17-s intervals: a 0–17 s, b 18–34 s, c 35–44 s, and d 45–54 s, for the model with longer slip-weakening distances (M3): smooth rupture front

is simplified, but it enables us to analyze patterns of slow and fast slips and other rupture characteristics, and to reveal relations between these patterns and underlying fault heterogeneities. Therefore, the model can be qualitatively interpreted in terms of a subduction megathrust with heterogeneous frictional coupling distribution.

Strong, coupled interface patches (asperities) and their weaker surroundings resulting from a variety of material and structural fault features, such as subducted seamounts or ridges, sediments, and released fluids, are modeled as respective distributions of frictional peak stresses and slip-weakening distances (Scholz and Campos 2012; Heuret et al. 2012; Vannucchi et al. 2017). The patches of high peak stresses are interpreted as asperities. The asperities have their internal structures: More or less densely distributed stronger places are surrounded by weaker ones (Uchida and Matsuzawa 2011). The asperities are characterized by different slip-weakening distances. Due to such asperity structure, the coseismic slip area depends on which of the strong sites break. Locked asperities limit the possible slip area size of other

asperities located within their areas. The largest earthquakes occur after the strongest asperity in a given region breaks. Then, weaker asperities start to define smaller rupture areas surrounding them (Senatorski 2017).

Healing processes are enabled if the driving stress drops below a threshold value. The fault does not heal under high driving stress, even if the net stress and the slip rate are low. Such an approach is motivated by subduction channel characteristics, where high driving stress inhibits underplating and enables erosion at the channel roof and the overriding plate. Thus, the healing mechanism is distinguished from the laboratory-derived friction law, which is adequate for a well-defined rupture plane. On the other hand, the stress-dependent healing can be also supported by laboratory experiments (Brantut 2015), where the proposed mechanism of the observed damage recovery is related to the microcrack closure. Further studies on the healing mechanism in the subduction channel context are needed.

The tectonic stress is understood as the uniform stress component in a major fault region. Cyclic

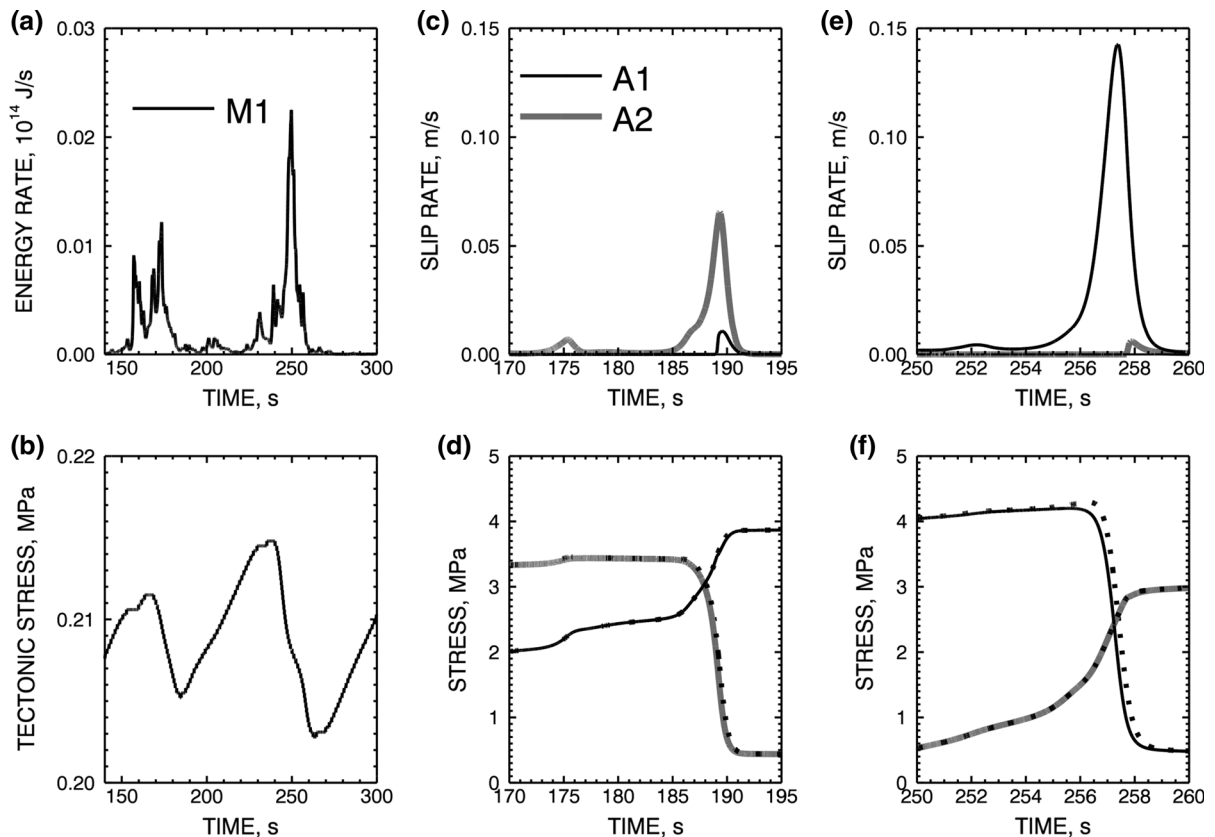


Figure 9

Simulated earthquake (M1). Temporal variations of the radiated energy rate (a), tectonic stress (b), slip velocities (c), and stresses (d) at A1 and A2 for the first and second (e and f, respectively) subevent. Dotted lines represent driving stresses and solid lines represent cohesive stresses (see Eq. 1)

stress accumulations and reliefs are reflected by vertical motions observed on the surface above megathrust seismogenic fault segments. Therefore, saw blade patterns of continuous GPS and sea level time series can be compared with the simulated tectonic stress variations (Natawidjaja et al. 2004; Sieh et al. 2008; Konca et al. 2008).

The present paper is focused on the role played by the slip-weakening distance values, d , in the stable vs. unstable slip interplay and large earthquake occurrences. Unlike in other papers (Hillers et al. 2006), distributions of d are not defined separately; instead, values of d are proportional to strengths, b , which define asperity distributions. Higher or lower d in models M1–M4 are related to their assumed maximum value.

Larger d values lead, on average, to higher tectonic stresses, but smaller stress drops, since stresses

decrease gradually to minimum stress levels. Thus, large d stabilizes the system. The model limits seismic activity to the fault plane only; in the real world, higher tectonic stresses may be responsible for higher seismicity levels in the surrounding fault.

Sequences of small or moderate earthquakes do not exclude large events. A great earthquake can occur after the toughest asperity breaks and a large-scale slip becomes possible. Analyses of the slip budget and rupture style of smaller earthquakes, assumed to be related to distribution of d , could be used to estimate the potential for large events. In the real world, sequences of moderate earthquakes occur within the Tohoku–Oki 2011 earthquake region (Hashimoto et al. 2012).

Large d values can both promote and restrain moderate or large earthquakes. Large events are promoted for two reasons, related to (1) the

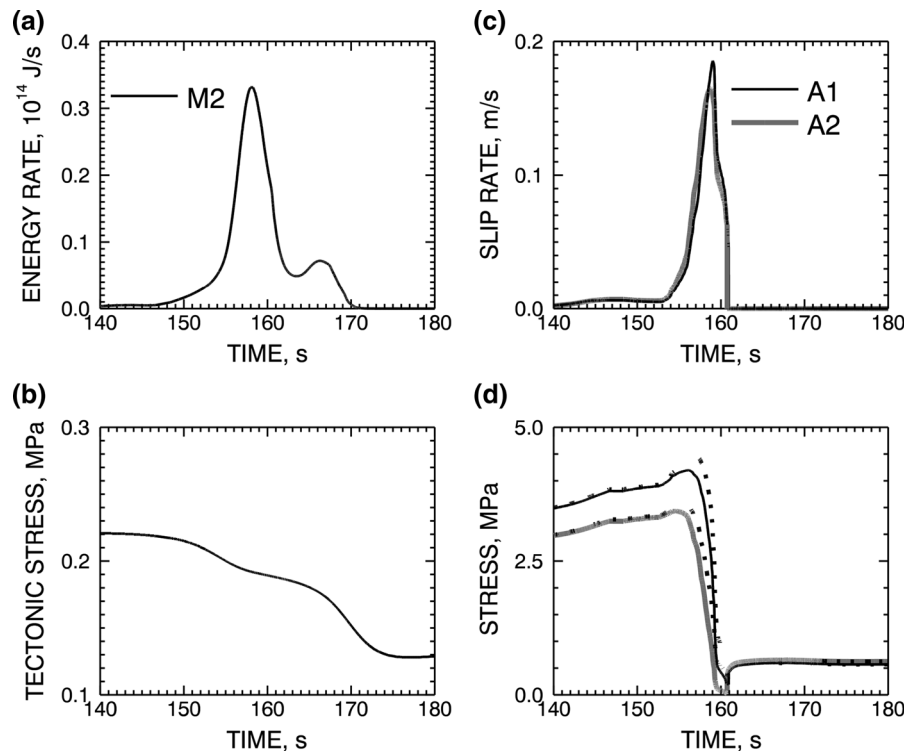


Figure 10

Simulated earthquake (M2). Temporal variations of the radiated energy rate (a), tectonic stress (b), slip velocities (c) and stresses (d) at A1 and A2. Dotted lines represent driving stresses and solid lines represent cohesive stresses (see Eq. 1)

system stiffness and (2) interaction strength. First, the unstable movements at the strongest asperities become possible only when the slipping area is large enough (so, the system stiffness becomes small enough), say larger than the asperity size. Second, a larger fault area is involved by the rupture process, because longer slips at instability imply higher stresses acting on neighboring asperities (so, interactions among asperities are stronger).

If, due to a large d value, individual asperities cannot release all the accumulated stresses by unstable slip, two scenarios are possible: (1) They break within a larger slipping area, or (2) they slip gradually by slow movements at high driving stresses. In the first case, the strong patches promote large events, as described above, accumulating stress for a long time. In the second case, however, they restrain large earthquakes. Depending on both strength and slip-weakening distance distributions, large events or aseismic creeping occur. The system can switch

between these two scenarios, if the distributions change due to some physical processes.

Small d values allow the same asperities to break singly. In this case, small and moderate earthquakes are promoted, depending on asperity sizes and the fault structure. This leads to the effect of stress switching at neighboring asperities that break one after another (Fig. 9). Large earthquakes, involving more asperities breaking in groups, are possible, but as a random effect: The asperities break together if they just happen to be in the same phase. For large d , asperities tend to break in groups, embracing large regions with both high and low strengths.

Possibility of different roles played by asperities, depending on the fault structure and its material characteristics, shed some light on the controversy about whether subducted seamounts start or stop large earthquakes (Mochizuki et al. 2008; Wang and Bilek 2011; Scholz and Campos 2012). Both roles can be played in the real world, and parameter d seems to be an important factor. The seamounts are

thought of as the regions of higher normal stresses, which enable unstable slips (Scholz and Small 1997). However, the slip-weakening distance, d , is another factor deciding the slip style besides strength. Thus, the subducted seamounts can play both roles, moving by unstable slips or creeping, depending on the material characteristics on the plate interface.

Both slow and fast slip movements are possible at the sites with large d values, depending on the slipping area size. Only slow slip is possible, if the size is limited by strong, locked asperities. Fast slip occurs after consecutive asperities break and the area of possible slip increases.

Large and smooth waves of the slip velocity field propagate into weaker segments that slip slowly otherwise. This effect explains the unstable slip at the shallow fault segment close to the trench during Tohoku–Oki 2011 earthquake.

The stiffness dependence on the slipping area size leads to a rupture hierarchy. Locked asperities cause the back stress in their surroundings and limit the possible slip area size of other asperities. Both stable and unstable slips are possible within the locked asperity region, but such slips become larger and faster after the locking site breaks. Such a view is consistent with the hierarchical asperity model outlined by Uchida and Matsuzawa (2011) and Lay (2015). According to that model, the plate frictional coupling is defined by hierarchical asperity structures. The present paper shows that the hierarchical megathrust nature may result both from heterogeneous frictional coupling, as well as the system dynamics dependent on changing stability conditions along the fault.

By using the quasi-dynamics approximation in simulations, inertial effects of the rupture process are neglected, as described in Sect. 2.1. Such effects can be important during large earthquakes, when the area of simultaneous slip is large and the rupture front propagates fast (Senatorski 2014). Their significance for the interplay between slow and fast fault movements, and for the fault stability conditions that lead to seismic or aseismic character of slip, is debatable. The present work is an attempt to find a possible explanation of the unexpected seismic–aseismic slip patterns without referring to the inertial effects.

5. Conclusions

The heterogeneous fault model with slip-dependent friction enables us to explain some unexpected seismicity patterns in subduction zones. The debated observations concern seismic and aseismic slips that occur at the same sites, hierarchical nature of the megathrust dynamics, and different roles played by subducted seamounts. Two related effects, the fault stiffness and slip-weakening distance, provide a key to understand these findings. The role of both effects have been often neglected. Although continuum fault models have inherently incorporated the fault stiffness, most works are focused on local friction law and its modifications only to explain the observed seismicity patterns.

The main findings can be summarized as follows.

- Complex processes within a subduction channel can be modeled by using the slip-dependent friction law with strength and slip-weakening distance as two model parameters.
- Slow or fast slip is more than the friction law problem only; it depends also on the changing system stiffness, which is related to the rupture area size.
- Relatively large slip-weakening distance value leads to a variety of slip patterns with both small and large earthquakes possible.

Future works should reveal specific relations between model parameters, such as strengths, slip-weakening distance and healing stress values, and subduction channel characteristics in the real world.

Acknowledgements

Constructive comments by the editor Sylvain Barbot and two anonymous reviewers helped me to improve the manuscript. This work was partially supported within statutory activities no. 3841/E-41/S/2018 of the Ministry of Science and Higher Education of Poland.

Open Access This article is distributed under the terms of the Creative Commons Attribution 4.0 International License (<http://creativecommons.org/licenses/by/4.0/>), which permits unrestricted use, distribution, and reproduction in any medium, provided you

give appropriate credit to the original author(s) and the source, provide a link to the Creative Commons license, and indicate if changes were made.

REFERENCES

- Achenbach, J. D. (1975). *Wave propagation in elastic solids*. Amsterdam: Elsevier Science Publishers B.V.
- Brantut, N. (2015). Time-dependent recovery of microcrack damage and seismic wave speeds in deformed limestone. *Journal of Geophysical Research: Solid Earth*, 120, 80888109. <https://doi.org/10.1002/2015JB012324>.
- Brune, J. N. (1970). Tectonic stress and the spectra of seismic shear waves from earthquakes. *Journal of Geophysical Research*, 75, 4997–5009.
- Brune, J.N. (1976). The physics of earthquake strong motion. In: Rosenbluthe, E., Lomnitz, C. (Eds.) *Seismic Risk And Engineering Decisions. Develop. in Geotech. Eng.*, 15.
- Chinnery, M. (1963). The stress changes that accompany strike-slip faulting. *Bulletin of the Seismological Society of America*, 53, 921–932.
- Cloos, M., & Shreve, R. L. (1988). Subduction-channel model of prism accretion, melange formation, sediment subduction, and subduction erosion at convergent plate margins: 1. Background and description. *Pure and Applied Geophysics*, 128, 455–499.
- Cloos, M., & Shreve, R. L. (1996). Shear zone thickness and the seismicity of Chilean- and Marianas-type subduction zones. *Geology*, 24, 107–110.
- Cochard, A., & Madariaga, R. (1994). Dynamic faulting under rate-dependent friction. *Pure and Applied Geophysics*, 142, 420–445.
- Day, S. M., Dalguer, L. A., Lapusta, N., & Liu, Y. (2005). Comparison of finite difference and boundary integral solutions to three-dimensional spontaneous rupture. *Journal of Geophysical Research*, 110, B12307. <https://doi.org/10.1029/2005JB003813>.
- Fukuyama, E., & Hok, S. (2013). Dynamic overshoot near trench caused by large asperity break at depth. *Pure and Applied Geophysics*. <https://doi.org/10.1007/s00024-013-0745-z>.
- Hashimoto, C., Noda, A., & Matsu'ura, M. (2012). The Mw 9.0 northeast Japan earthquake: total rupture of a basement asperity. *Geophysical Journal International*, 189(1), 1–5. <https://doi.org/10.1111/j.1365-246X.2011.05368.x>.
- Heuret, A., Conrad, P., Funicicello, F., Lallemand, S., & Sandri, L. (2012). Relation between subduction megathrust earthquakes, trench sediment thickness and upper plate strain. *Geophysical Research Letters*, 39, L05304. <https://doi.org/10.1029/2011GL050712>.
- Hillers, L., Ben-Zion, Y., & Mai, P. M. (2006). Seismicity on a fault controlled by rate- and state-dependent friction with spatial variations of the critical slip distance. *Journal of Geophysical Research*, 111, B01403. <https://doi.org/10.1029/2005JB003859>.
- Hirth, J. P., & Lothe, J. (1967). *Theory of Dislocations*. New York: McGraw-Hill.
- Huang, Y., Ampuero, J.-P., & Kanamori, H. (2013). Slip-weakening Models of the Tohoku-Oki earthquake and constraints on stress drop and fracture energy. *Pure and Applied Geophysics*, 171, 2555–25668.
- Ide, S., Baltay, A., & Beroza, G. C. (2011). Shallow Dynamic Overshoot and Energetic Deep Rupture in the 2011 Mw 9.0 Tohoku-Oki Earthquake. *Science*, 332, 1426. <https://doi.org/10.1126/science.1207020>.
- Johnson, K. M., Fukuda, J., & Segall, P. (2012). Challenging the rate-state asperity model: Afterslip following the 2011 M9 Tohoku-oki, Japan, earthquake. *Geophysical Research Letters*, 39, L20302. <https://doi.org/10.1029/2012GL052901>.
- Konca, A. O., Jean-Philippe Avouac, J.-P., Sladen, A., Meltzner, A. J., Sieh, K., Fang, P., et al. (2008). Partial rupture of a locked patch of the Sumatra megathrust during the 2007 earthquake sequence. *Nature*, 456, 631–635.
- Lay, T. (2015). The surge of great earthquakes from 2004 to 2014. *Earth and Planetary Science Letters*, 409, 133–146.
- Lay, T., Kanamori, H., & Ruff, L. (1982). The asperity model and the nature of large subduction zone earthquake occurrence. *Earthquake Prediction Research*, 1, 3–71.
- Lichtenberg, A.J., & Lieberman, M.A. (1992). *Regular and chaotic dynamics*, 2nd edn., Applied Mathematical Sciences, series vol. 38, Springer, New York.
- Loveless, J. P., & Meade, B. J. (2011). Spatial correlation of interseismic coupling and coseismic rupture extent of the 2011 MW = 9.0 Tohoku-oki earthquake. *Geophysical Research Letters*, 38, L17306. <https://doi.org/10.1029/2011GL048561>.
- Mansinha, L., & Smylie, D. E. (1971). The displacement field of inclined faults. *Bulletin of the Seismological Society of America*, 61, 1433–1440.
- Mochizuki, K., Yamada, T., Shinohara, M., Yamanaka, Y., & Kanazawa, T. (2008). Weak Interplate Coupling by Seamounts and Repeating M 7 Earthquakes. *Science*, 321, 1194–1197.
- Moreno, M., Rosenau, M., & Oncken, O. (2010). 2010 Maule earthquake slip correlates with pre-seismic locking of Andean subduction zone. *Nature*, 467, 198–202.
- Moreno, M., Melnick, D., Rosenau, M., Baez, J., Klotz, J., Oncken, O., et al. (2012). Toward understanding tectonic control on the Mw 8.8 2010 Maule Chile earthquake. *Earth and Planetary Science Letters*, 321–322, 152–165.
- Natawidjaja, D. H., Sieh, K., Ward, S. N., Cheng, H., Edwards, R. L., Suwargadi, B. W., et al. (2004). Paleogeodetic records of seismic and aseismic subduction from central Sumatran microatolls, Indonesia. *Geophysical Research Letters*, 109, B04306. <https://doi.org/10.1029/2003JB002398>.
- Noda, H., & Lapusta, N. (2013). Stable creeping fault segments can become destructive as a result of dynamic weakening. *Nature*, 493, 518–521.
- Ohnaka, M. (2013). *The Physics of Rock Failure and Earthquakes*. New York: Cambridge University Press.
- Ohnaka, M., & Shen, L. (1999). Scaling of the shear rupture process from nucleation to dynamic propagation: implications of geometric irregularity of the rupturing surfaces. *Journal of Geophysical Research*, 104, 817–844.
- Ohtani, M., Hirahara, K., Hori, T., & Hyodo, M. (2014). Observed change in plate coupling close to the rupture initiation area before the occurrence of the 2011 Tohoku earthquake: Implications from an earthquake cycle model. *Geophysical Research Letters*, 41, 1899–1906. <https://doi.org/10.1002/2013GL058751>.
- Ohtani, M., & Hirahara, K. (2015). Effect of the Earths surface topography on quasi-dynamic earthquake cycles. *Geophysical Journal International*, 203, 384–398.
- Okada, Y. (1992). Internal deformation due to shear and tensile faults in a half-space. *Bulletin of the Seismological Society of America*, 82, 1018–1040.

- Peng, Z., & Gomberg, J. (2010). An integrated perspective of the continuum between earthquakes and slow-slip phenomena. *Nature Geoscience*, 3, 599–607.
- Rice, J. R. (1993). Spatio-temporal complexity of slip on a fault. *Journal of Geophysical Research*, 98, 9885–9907.
- Rundle, J. B. (1989). A physical model for earthquakes: 3. Thermodynamical approach and its relation to nonclassical theories of nucleation. *Journal of Geophysical Research*, 94, 2839–2855.
- Scholz, C. H., & Small, C. (1997). The effect of seamount subduction on seismic coupling. *Geology*, 25, 487–490. <https://doi.org/10.1130/0091-7613>.
- Scholz, C. H., & Campos, J. (2012). The seismic coupling of subduction zones revisited. *Journal of Geophysical Research*, 117, B05310. <https://doi.org/10.1029/2011JB009003>.
- Senatorski, P. (1994). Spatio-temporal evolution of faults: deterministic model. *Physica D*, 76, 420–435.
- Senatorski, P. (1995). Dynamics of a zone of four parallel faults: A deterministic model. *Journal of Geophysical Research*, 100, 24111–24120.
- Senatorski, P. (2002). Slip-weakening and interactive dynamics of an heterogeneous seismic source. *Tectonophysics*, 344, 37–60.
- Senatorski, P. (2004). Interactive dynamics of an heterogeneous seismic source. A model with the slip dependent friction. *Pub. Inst. Geophys. PAS, A-27(354)*, Monographic Vol., pp.151.
- Senatorski, P. (2006). Fluctuations, trends and scaling of the energy radiated by heterogeneous seismic sources. *Geophysical Journal International*, 166, 267–276.
- Senatorski, P. (2008). Apparent stress scaling for tectonic and induced seismicity: Model and observations. *Physics of the Earth and Planetary Interiors*, 167, 98–109.
- Senatorski P. (2014). Radiated energy estimations from finite-fault earthquake slip models. *Geophysical Research Letters*. <https://doi.org/10.1002/2014GL060013>.
- Senatorski, P. (2017). Effect of slip-area scaling on the earthquake frequency-magnitude relationship. *Physics of the Earth and Planetary Interiors*, 267, 41–52.
- Sieh, K., Natawidjaja, D. H., Meltzner, A. J., Shen, C.-C., Cheng, H., Li, K.-S., et al. (2008). Earthquake supercycles inferred from sea-level changes recorded in the Corals of West Sumatra. *Science*, 322, 1674–1678.
- Stoyan, D., Kendall, W. S., & Mecke, J. (1995). *Stochastic Geometry and its Applications* (2nd ed.). Chichester: Wiley.
- Thomas, M. Y., Lapusta, N., & Avouac, J.-P. (2014). Quasi-dynamic versus fully dynamic simulations of earthquakes and aseismic slip with and without enhanced coseismic weakening. *Journal of Geophysical Research: Solid Earth*, 119, 1986–2004. <https://doi.org/10.1002/2013JB010615>.
- Turcotte, D. L. (1997). *Fractals and Chaos in Geology and Geophysics* (2nd ed.). New York: Cambridge University Press.
- Uchida, N., & Matsuzawa, T. (2011). Coupling coefficient, hierarchical structure, and earthquake cycle for the source area of the 2011 off the Pacific coast of Tohoku earthquake inferred from small repeating earthquake data. *Earth Planets Space*, 63, 675–679. <https://doi.org/10.5047/eps.2011.07.006>.
- Vannucchi, P., Sage, F., Phipps Morgan, J., Remitti, F., & Collot, J.-Y. (2012). Toward a dynamic concept of the subduction channel at erosive convergent margin with implications for interplate material transfer. *Geochemistry, Geophysics, Geosystems*, 13, Q02003. <https://doi.org/10.1029/2011GC003846>.
- Vannucchi, P., Spagnuolo, E., Aretusini, S., Di Toro, G., Ujiie, K., Tsutsumi, A., et al. (2017). Past seismic slip-to-the-trench recorded in Central America megathrust. *Nature Geoscience*, 10, 935–940. <https://doi.org/10.1038/s41561-017-0013-4>.
- Wang, K., & Bilek, S. L. (2011). Do subducting seamounts generate or stop large earthquakes? *Geology*, 39, 819–822. <https://doi.org/10.1130/G31856.1>.
- Ziv, A., & Cochard, A. (2006). Quasi-dynamic modeling of seismicity on a fault with depth-variable rate- and state-dependent friction. *Journal of Geophysical Research*, 111, B08310. <https://doi.org/10.1029/2005JB004189>.

(Received January 29, 2018, revised October 1, 2018, accepted January 8, 2019, Published online January 22, 2019)